Multiantenna spectrum sensing exploiting spectral *a priori* information

Gonzalo Vazquez-Vilar*, *Student Member, IEEE*, Roberto López-Valcarce*, *Member, IEEE*, Josep Sala†, *Senior Member, IEEE*

* Dept. of Signal Theory and Communications, Universidad de Vigo
36310 Vigo, Spain. E-mail: {gvazquez,valcarce}@gts.uvigo.es

† Dept. of Signal Theory and Communications, Technical University of Catalonia (UPC)
c/Jordi Girona 1-3, Campus Nord UPC, 08034 Barcelona, Spain. E-mail: josep.sala@upc.edu

Abstract

Dynamic Spectrum Access (DSA) is receiving considerable interest as a means to improve spectral usage in licensed bands. In order to avoid interference to licensed users, spectrum sensing has emerged as an enabling technology for DSA. The requirements for spectrum sensors are stringent, as licensed user detection must be performed reliably at low signal-to-noise ratios (SNR). Sensing performance can be improved by exploiting signal features not present in the background noise. These approaches result in tradeoffs among performance and robustness to departures from the signal model. We consider second-order signal features and develop detectors exploiting spatial (by using multiple antennas) as well as temporal signal correlation, taking advantage of the fact that the power spectrum of the primary signal at each antenna can be known up to a complex scalar representing the unknown propagation channel. A low-SNR Generalized Likelihood Ratio approach is adopted in order to overcome this uncertainty, resulting in different tests intimately related to familiar diversity combining techniques. The performance of the proposed detectors is analyzed and tested in different scenarios.

I. Introduction

The wireless community is showing considerable interest in the development of Dynamic Spectrum Access (DSA) techniques as a means to alleviate the apparent scarcity of spectral resources as perceived nowadays [2], [3]. DSA adoption will require powerful spectrum sensing schemes in order to allow the usage of spectral holes while maintaining the interference produced to licensed (primary) users at sufficiently low levels. Wireless propagation phenomena such as shadowing and fading pose significant challenges to the reliable detection of primary users. The received primary signal may be very weak, resulting in very low Signal-to-Noise Ratio (SNR) operation conditions

Research supported by the Spanish Government and the European Regional Development Fund (ERDF) under projects DYNACS (TEC2010-21245-C02/TCM) and COMONSENS (CONSOLIDER-INGENIO 2010 CSD2008-00010), and the Catalan Science & Technology Comission (AGAUR) under project 2009SGR1236. Parts of this work were presented at the 4th International Conference on Cognitive Radio Oriented Wireless Networks and Communications (CrownCom 2009), Hannover, Germany, June 2009 [1].

and "hidden node" situations. Cooperative sensing has the potential to overcome the effects of shadowing [4], [5], though it still relies on standalone detectors whose performance should be optimized.

Depending on the amount of information available about the structure of the primary signal, different detectors may be designed. Exploiting specific signal features (e.g. training sequences, cyclostationarity [6], [7], presence of a cyclic prefix [8], constant envelope [9], or spectrum shape [10]–[13]), it is possible to improve detection performance with respect to simpler approaches which do not attempt to model the primary signal, such as energy detection [14].

Since feature-based detectors tend to be sensitive to clock synchronization errors [15], our focus is on detectors based on knowledge about the spectral shape of primary transmissions. The resulting schemes do not require time synchronization with a potentially present signal (a difficult task in very low SNR conditions) and are quite general since no particular features of the primary signal are exploited beyond knowledge of its second-order statistics. In addition, we consider the use of multiple antennas at the spectrum monitoring device. In this way, spatial correlation in the received primary signal can be used to enhance detection performance. Hence the main contribution of this work is to consider jointly *temporal* and *spatial* signal correlation, under the assumption that noise is temporally and spatially white.

Previous work on multiantenna spectrum sensing is mainly based on spatial correlation only [16]–[18] and does not assume (or exploit) any information about the spectral shape of the primary signal. Under the assumption that the power spectral density (psd) of the signal is completely known, [19] derives the optimal Neyman-Pearson detector for both scalar and vector-valued signals. However, in spectrum sensing applications the propagation channel is unknown, and thus only partial knowledge of the second order statistics is available in practice. A possible approach in that case is to neglect this partial knowledge, and consider test statistics that quantify the departure of the sample temporal autocorrelation matrix of the observations from a scaled identity [12]. Alternatively, metrics quantifying the distance of the sample correlation matrix from a "candidate" matrix summarizing *a priori* knowledge can be used: in the single antenna setting, for example, [10] assumes the signal psd known up to a scaling and a shift, respectively modeling uncertainty about the power level and carrier frequency of the signal. Also assuming a single antenna, [13] adopts a similar approach when the carrier frequency is known, as it often occurs in practice: for instance, for frequency division multiple access (FDMA) primary networks with public channelization parameters.

In this work we generalize the approach from [13] to the multiple antenna setting. The channel gains from the primary transmitter to the sensor antennas are assumed unknown. A Generalized Likelihood Ratio (GLR) approach [20] for low SNR will be used to sidestep this problem, and different multiantenna detectors will be obtained in this way depending on the assumptions adopted. These detectors bear close relationship with several well-known diversity combining techniques from the communications field [21]. We present statistical analyses showing how these detectors offer different tradeoffs between complexity and performance.

The paper is organized as follows. The system model is introduced in Section II and the corresponding Hypothesis Testing Problem is discussed in Section III. Under different assumptions on the channel gains, in Section IV we derive the corresponding detectors and present theoretical performance analyses. Simulation results in diverse settings

are presented in Section V and final conclusions are drawn in Section VI.

Notation: lower and uppercase boldface symbols denote vectors and matrices, respectively. The vector of all ones is denoted by $\mathbf{1}$. The Kronecker product of $\boldsymbol{A}$ and $\boldsymbol{B}$ is denoted by $\boldsymbol{A} \otimes \boldsymbol{B}$. We use $\boldsymbol{y} \sim \mathcal{CN}(\boldsymbol{\mu}, \boldsymbol{P})$ to indicate that $\boldsymbol{y}$ is circularly complex Gaussian with mean $\boldsymbol{\mu}$ and covariance $\boldsymbol{P}$. Neper's base-e logarithm is denoted by $\log$. The Q-function (tail probability of the standard normal distribution) is defined as $Q(x) \doteq \frac{1}{\sqrt{2\pi}} \int_x^\infty \mathrm{e}^{-\frac{t^2}{2}} \mathrm{d}t$.

II. System model

An FDMA-based primary system with fixed channelization is assumed. The spectrum monitor is equipped with M antennas with their respective Radio Frequency (RF) chains. A given primary channel is selected, downconverted to baseband, and sampled at a rate f_s to obtain K complex-valued samples at each antenna ($T = K/f_s$ is the observation time). The samples at the m-th antenna are collected into the $K \times 1$ vector $\boldsymbol{y}_m$, given by

$$\boldsymbol{y}_m = \tilde{h}_m \boldsymbol{x} + \sigma_m \boldsymbol{w}_m, \qquad 1 \le m \le M, \tag{1}$$

where

- $\boldsymbol{x} = [\, x_0 \; x_1 \; \cdots \; x_{K-1} \,]^T$ comprises the samples of the primary signal.
- $\tilde{h}_m$ is the (unknown) complex channel gain at antenna m. If the channel is vacant, then $\tilde{h}_m = 0$ for all m.
- $\sigma_m^2 > 0$ is the noise variance at antenna m, assumed known.
- The noise is assumed temporally white and statistically independent across antennas: $E\{\boldsymbol{w}_m \boldsymbol{w}_n^H\} = \delta_{mn} \boldsymbol{I}_K$.

Since the noise variances are known, the observation at antenna m can be scaled to obtain

$$r_m = \frac{1}{\sigma_m} \boldsymbol{y}_m = h_m \boldsymbol{x} + \boldsymbol{w}_m, \tag{2}$$

where $h_m \doteq \tilde{h}_m / \sigma_m$. By introducing the vectors

$$\boldsymbol{r} \doteq \begin{bmatrix} \boldsymbol{r}_1 \\ \vdots \\ \boldsymbol{r}_M \end{bmatrix}, \quad \boldsymbol{w} \doteq \begin{bmatrix} \boldsymbol{w}_1 \\ \vdots \\ \boldsymbol{w}_M \end{bmatrix}, \quad \boldsymbol{h} \doteq \begin{bmatrix} h_1 \\ \vdots \\ h_M \end{bmatrix}, \tag{3}$$

the model (1) can be compactly written as

$$\boldsymbol{r} = \boldsymbol{h} \otimes \boldsymbol{x} + \boldsymbol{w}. \tag{4}$$

In order to protect primary users from interference, the operational range of spectrum sensors must include primary signals well below decodability levels; in such situations, attempting to synchronize with the potentially present primary signal is unrealistic. Thus, in a first approximation, $\{x_k\}$ can be assumed zero-mean wide-sense stationary with psd $S_{xx}(\mathrm{e}^{\jmath\omega})$, and normalized to unit power, i.e. $E\{|x_k|^2\} = \frac{1}{2\pi} \int_{-\pi}^{\pi} S_{xx}(\mathrm{e}^{\jmath\omega}) \mathrm{d}\omega = 1$. The average SNR per antenna, denoted by ρ, is therefore

$$\rho \doteq \frac{1}{M} \sum_{m=1}^{M} \frac{|\tilde{h}_m|^2}{\sigma_m^2} = \frac{||\boldsymbol{h}||_2^2}{M}. \tag{5}$$

We adopt a Gaussian model for the primary signal, for the following reasons. First, since the noise is assumed Gaussian as well, the Gaussian pdf for the signal is the least informative one for the detection problem. Second,

if the primary system uses multicarrier modulation with a reasonable number of subcarriers, the Gaussian model is quite accurate. Third, low-SNR approximations of the log-likelihood in ML estimation for general distribution of the signal of interest usually lead to detectors based on second-order statistics. The detectors proposed in the sequel are functions of sample correlations, and therefore, as the SNR goes to zero, the choice of the (Gaussian) distribution is not so relevant. And finally, this model is tractable and leads to useful detectors even if the Gaussian assumption does not hold, as will be shown in the simulation results. Therefore, it is assumed that $\boldsymbol{x} \sim \mathcal{CN}(\boldsymbol{0}, \boldsymbol{C})$, where $\boldsymbol{C} \doteq E\{\boldsymbol{x}\boldsymbol{x}^H\}$. Provided that the channelization parameters of the primary system are public (as will be the case for e.g. broadcast networks, cellular networks, etc.), then $S_{xx}(\mathrm{e}^{\jmath\omega})$ is known (and so is $\boldsymbol{C}$). Note that $\boldsymbol{C}$ is Toeplitz with ones on the diagonal. In general, $\{x_k\}$ will be colored (and $\boldsymbol{C} \neq \boldsymbol{I}_K$) as a result of interchannel guard bands, pulse shaping, etc.

Let $\boldsymbol{C} = \boldsymbol{U}\boldsymbol{\Lambda}\boldsymbol{U}^H$ with $\boldsymbol{\Lambda} = \mathrm{diag}(\lambda_0\ \lambda_1\ \cdots\ \lambda_{K-1})$ be an eigendecomposition of $\boldsymbol{C}$, and let $\boldsymbol{W}$ be the $K \times K$ orthonormal IDFT matrix. It is well known [20] that as $K \to \infty$ (long observation time), the eigenvectors and eigenvalues of $\boldsymbol{C}$ can be approximated as

$$\boldsymbol{U} \to \boldsymbol{W}, \qquad \lambda_k \to S_{xx}(\mathrm{e}^{\jmath\frac{2\pi k}{K}}), \quad 0 \leq k \leq K-1, \tag{6}$$

which can be formally justified in terms of the asymptotic equivalence between sequences of matrices and the asymptotic eigenvalue distribution of circulant and Toeplitz matrices [22]. The following *spectral shape parameters* will feature in the statistical analysis of the detectors:

$$\bar{b}_n \doteq \frac{1}{K}\,\mathrm{tr}\{\boldsymbol{C}^n\} \quad = \quad \frac{1}{K}\sum_{k=0}^{K-1}\lambda_k^n \tag{7}$$

$$\approx \quad \frac{1}{2\pi}\int_{-\pi}^{\pi} S_{xx}^n(\mathrm{e}^{\jmath\omega})d\omega \quad \text{for } K \to \infty. \tag{8}$$

Note that $\bar{b}_1 = 1$ since $\mathrm{E}\{|x_k|^2\} = 1$. For white $\{x_k\}$, $\boldsymbol{C} = \boldsymbol{I}_K$ so that $\bar{b}_n = 1$ for all n (in general, one has $\bar{b}_n \geq 1$ by Jensen's inequality).

III. Multiantenna detection

Based on the $MK \times 1$ vector $\boldsymbol{r}$ from (4), and under the Gaussian model, the corresponding hypothesis test is

$$\begin{aligned} \mathcal{H}_0 &: \quad \boldsymbol{r} \sim \mathcal{CN}(\boldsymbol{0}, \mathcal{R}_0) \qquad \text{(primary is absent)} \\ \mathcal{H}_1 &: \quad \boldsymbol{r} \sim \mathcal{CN}(\boldsymbol{0}, \mathcal{R}_1) \qquad \text{(primary is present)} \end{aligned} \tag{9}$$

where $\mathcal{R}_0 \doteq \boldsymbol{I}_{MK}$ and $\mathcal{R}_1 \doteq \boldsymbol{I}_{MK} + \mathcal{G}$, with

$$\mathcal{G} \doteq \mathcal{R}_1 - \mathcal{R}_0 = \boldsymbol{h}\boldsymbol{h}^H \otimes \boldsymbol{C}. \tag{10}$$

The Neyman-Pearson (NP) test for this Gaussian detection problem is an estimator-correlator [20] declaring $\mathcal{H}_1$ true if $\boldsymbol{r}^H\hat{\boldsymbol{z}}$ exceeds a threshold, where $\hat{\boldsymbol{z}}$ is the minimum mean squared error (MMSE) estimator of $\boldsymbol{z} \doteq \boldsymbol{h} \otimes \boldsymbol{x}$ given $\boldsymbol{r}$ and $\boldsymbol{h}$, and it is given by $\hat{\boldsymbol{z}} = \mathcal{G}\mathcal{R}_1^{-1}\boldsymbol{r}$. Note that this test requires knowledge of $\boldsymbol{h}\boldsymbol{h}^H$.

At this point it is instructive to review the single-antenna case [13]. If $M = 1$, then $\mathcal{G} = |h|^2\boldsymbol{C} = \rho\boldsymbol{C}$, and the NP test statistic can be written as

$$\boldsymbol{r}^H\hat{\boldsymbol{z}} = \sum_{k\in\mathcal{B}} \frac{\rho\lambda_k}{1+\rho\lambda_k}|v_k|^2, \tag{11}$$

where $\boldsymbol{v} = [v_0\, v_1\, \cdots\, v_{K-1}]^T \doteq \boldsymbol{U}^H\boldsymbol{r}$, so that $\mathcal{B} \subset \{0, 1, \ldots, K-1\}$ is the set of indices of nonzero eigenvalues of $\boldsymbol{C}$. In view of (6), for large K one has $\boldsymbol{v} \approx \boldsymbol{W}^H\boldsymbol{r}$ (the DFT of the observations), and $\mathcal{B}$ is the support of $\lambda_k \approx S_{xx}(\mathrm{e}^{\jmath\frac{2\pi k}{K}})$. Thus (11) is just the correlation between the periodogram $\{|v_k|^2\}$ and the SNR-dependent spectral mask $\{\rho\lambda_k/(1+\rho\lambda_k)\}$. In the following asymptotic cases, the NP test becomes independent of ρ:

- High SNR case: if $\rho\lambda_k \gg 1$ for all $k \in \mathcal{B}$, then $\boldsymbol{r}^H\hat{\boldsymbol{z}} \approx \sum_{k\in\mathcal{B}}|v_k|^2$. Thus the NP test reduces to an Energy Detector (ED) over the spectral support of the primary signal. If $\boldsymbol{C}$ is full rank, then $\boldsymbol{r}^H\hat{\boldsymbol{z}} \approx \boldsymbol{v}^H\boldsymbol{v} = \boldsymbol{r}^H\boldsymbol{r}$, i.e. the standard energy detector.
- Low SNR case: if $\rho\lambda_k \ll 1$ for all $k \in \mathcal{B}$, then the NP test declares $\mathcal{H}_1$ true if $\sum_{k\in\mathcal{B}}\lambda_k|v_k|^2 = \boldsymbol{r}^H\boldsymbol{C}\boldsymbol{r}$ exceeds a threshold. This is also the *Locally Most Powerful* (LMP) test for this problem, derived from weak signal detection theory [20], and which does make use of the available information about the primary signal spectrum, in contrast with the ED test.

However, with $M > 1$ antennas, neither in the high nor low SNR regimes does the dependence of the NP test with $\boldsymbol{h}\boldsymbol{h}^H$ disappear. In the sequel, we will focus on the case of asymptotically small SNR, which is of more relevance in spectrum sensing applications. Then, using $\mathcal{R}_1^{-1} \approx \boldsymbol{I}_{MK}$, one has

$$\begin{aligned}
\boldsymbol{r}^H\hat{\boldsymbol{z}} &\approx \boldsymbol{r}^H(\boldsymbol{h}\boldsymbol{h}^H \otimes \boldsymbol{C})\boldsymbol{r} && (12)\\
&= \sum_{i=1}^{M}\sum_{j=1}^{M} \boldsymbol{r}_i^H(h_i h_j^*\boldsymbol{C})\boldsymbol{r}_j && (13)\\
&= \boldsymbol{s}^H\boldsymbol{C}\boldsymbol{s} \doteq T_0, && (14)
\end{aligned}$$

where we have introduced

$$\boldsymbol{s} = \boldsymbol{s}_{\text{MRC}} \doteq \sum_{l=1}^{M} h_l^*\boldsymbol{r}_l. \tag{15}$$

As in the single-antenna case, T_0 can be interpreted as a frequency-domain correlation, but now between the spectral mask $\{\lambda_k\}$ and the squared magnitude of the DFT of a linear combination $\boldsymbol{s}$ of the signals at the antennas. We use the subscript MRC since this processing is akin to the *Maximal Ratio Combining* technique for diversity recepcion [21], by which the signals collected at each of the antennas are phased-aligned and combined with optimal weighting to maximize the SNR at the combiner output and prior to the demodulation stage (incidentally, when the signal of interest is white, i.e. $\boldsymbol{C} = \boldsymbol{I}_K$, then the decision rule $T_0 = \boldsymbol{s}^H\boldsymbol{s} \gtrless \gamma$ is optimal for all SNR values [16]). Note that the computation of the NP test statistic for low SNR only requires knowledge of the spherical component $\bar{\boldsymbol{h}} \doteq \boldsymbol{h}/\|\boldsymbol{h}\|_2$. The threshold can be set to achieve a given false alarm rate under $\mathcal{H}_0$, i.e. under $\|\boldsymbol{h}\|_2 = 0$.

Note now that if we neglect the magnitude gains of the coefficients h_l^* in (15), then $\boldsymbol{s}$ can be approximated as

$$\boldsymbol{s} \approx \boldsymbol{s}_{\text{EGC}} \doteq \sum_{l=1}^{M} \mathrm{e}^{-\jmath\theta_l} \boldsymbol{r}_l \tag{16}$$

where $\theta_l \doteq \arg\{h_l\}$. This is analogous to the *Equal Gain Combining* (EGC) [21]. One can also approximate $\boldsymbol{s}$ by the signal at the branch with highest SNR as is done in *Selection Combining* (SC) [21]:

$$\boldsymbol{s} \approx \boldsymbol{s}_{\text{SC}} \doteq \boldsymbol{r}_m \quad \text{with} \quad m = \underset{1\le i\le M}{\arg\max}\, |h_i|^2. \tag{17}$$

Note that if all branches have similar SNRs, then $\boldsymbol{s}_{\text{MRC}} \approx \boldsymbol{s}_{\text{EGC}}$. On the other hand, when the SNR at one of the antennas is much larger than the rest, then $\boldsymbol{s}_{\text{MRC}} \approx \boldsymbol{s}_{\text{SC}}$.

However, none of these schemes (MRC, EGC and SC) is directly implementable, since they depend on unknown channel parameters. In the next section different paths around this problem are presented. Inspired by the Generalized Likelihood Ratio (GLR) approach, the Maximum Likelihood (ML) estimates of the unknown parameters can be obtained under different assumptions; substituting these ML estimates in the corresponding statistics will in turn yield a variety of practical detectors.

IV. Parameter estimation and detection

In order to derive ML estimates of the unknown parameters under different models, note that the negative of the log–likelihood function under $\mathcal{H}_1$ is given by $-\log f(\boldsymbol{r}\,|\,\boldsymbol{h}) = \log\det(\boldsymbol{I}+\mathcal{G}) + \boldsymbol{r}^H(\boldsymbol{I}+\mathcal{G})^{-1}\boldsymbol{r}$, where $\mathcal{G}$ depends on $\boldsymbol{h}$ as per (10). In the low SNR regime, we can approximate $[\boldsymbol{I}+\mathcal{G}]^{-1} \approx \boldsymbol{I}-\mathcal{G}$ and $\log\det(\boldsymbol{I}+\mathcal{G}) \approx \operatorname{tr}\mathcal{G}$ (using the fact that $\log(1+x)\approx x$ for small $|x|$). Thus, noting that $\operatorname{tr}\mathcal{G} = (\operatorname{tr}\boldsymbol{h}\boldsymbol{h}^H)(\operatorname{tr}\boldsymbol{C}) = \|\boldsymbol{h}\|_2^2 K$, the following low–SNR approximation is obtained:

$$-\log f(\boldsymbol{r}\,|\,\boldsymbol{h}) \approx K\|\boldsymbol{h}\|_2^2 + \|\boldsymbol{r}\|_2^2 - \boldsymbol{r}^H\mathcal{G}\boldsymbol{r}. \tag{18}$$

A. Generalized energy detector

The simplest multiantenna detector disregards antenna crosscorrelation and assumes equal weighting for the energy estimates at the different antennas. The statistic (14) of the low-SNR NP test can be writen as

$$T_0 = \sum_{i=1}^{M}\sum_{j=1}^{M} h_i h_j^* \boldsymbol{r}_i^H \boldsymbol{C}\boldsymbol{r}_j. \tag{19}$$

If we ignore the terms depending on $h_i h_j^*$ for $i \neq j$, phase alignment is no longer required. If we further assume $|h_i| \approx |h_j|$ for $i \neq j$, and with γ_{GED} a threshold, the corresponding decision rule reduces to

$$T_{\text{GED}} \;=\; \sum_{i=1}^{M} \boldsymbol{r}_i^H \boldsymbol{C}\boldsymbol{r}_i \underset{\mathcal{H}_0}{\overset{\mathcal{H}_1}{\gtrless}} \gamma_{\text{GED}}, \tag{20}$$

We refer to the test (20) as "Generalized Energy Detector" (GED), as it merely collects the (spectrally weighted) energy from all branches. This detector can be used in distributed settings with M collaborating single-antenna sensors: each node reports its local statistic $\boldsymbol{r}_i^H\boldsymbol{C}\boldsymbol{r}_i$ to a Fusion Center, where all such statistics are added together.

The asymptotic performance of this detector is analyzed in Appendix A, showing that for sufficiently large K, the threshold γ_{GED} can be selected in order to achieve a prespecified false alarm rate P_{FA} as

$$\gamma_{\text{GED}} = KM\left[1+\sqrt{\frac{\bar{b}_2}{KM}}Q^{-1}(P_{\text{FA}})\right], \tag{21}$$

and the resulting probability of detection is given by

$$P_{\text{D}}^{\text{GED}} = Q\left(\frac{Q^{-1}(P_{\text{FA}})-\sqrt{KM\bar{b}_2}\rho}{\sqrt{M\frac{\bar{b}_4}{\bar{b}_2}\rho^2+2\frac{\bar{b}_3}{\bar{b}_2}\rho+1}}\right). \tag{22}$$

Note that GED performance depends only on the average SNR ρ, but not on the spherical component $\bar{\boldsymbol{h}} = \boldsymbol{h}/\|\boldsymbol{h}\|_2$.

B. Selection Combining detector

The SC detector is based on the approximation (17), and thus requires the estimation of the index m of the antenna with largest SNR. In the general case, ML estimation of this index is not tractable, and thus we resort to the low SNR approximation (18); in addition, we will assume that $\boldsymbol{h} = h\boldsymbol{e}_m$, where $\boldsymbol{e}_m$ is the m-th unit vector. The reason for this is that, as mentioned above, the SC approach is expected to provide close-to-optimal performance in scenarios in which the SNR at one of the antennas is dominant.

Under this assumption, one has $\|\boldsymbol{h}\|_2^2 = |h|^2$ and $\boldsymbol{r}^H\mathcal{G}\boldsymbol{r} = |h|^2\boldsymbol{r}_m^H\boldsymbol{C}\boldsymbol{r}_m$ in (18). Therefore, the ML estimate of m is just $\hat{m} = \arg\max_m \boldsymbol{r}_m^H\boldsymbol{C}\boldsymbol{r}_m$. The resulting decision rule is given by

$$T_{\text{SC}} \doteq \max_{1\le m\le M} \boldsymbol{r}_m^H\boldsymbol{C}\boldsymbol{r}_m \underset{\mathcal{H}_0}{\overset{\mathcal{H}_1}{\gtrless}} \gamma_{\text{SC}}. \tag{23}$$

Thus, the SC detector picks the antenna with largest spectrally weighted SNR and uses that SNR as statistic. Note that this amounts to an OR fusion rule, and can be applied in distributed settings: the channel is declared busy if the spectrally weighted SNR at any of the M nodes exceeds a threshold. In that case, only one bit of information has to be sent to the Fusion Center by each node, in contrast with the GED scheme.

The asymptotic performance of the SC detector is discussed in Appendix B. For large K, the local threshold γ_{SC} that yields global false alarm rate P_{FA} is

$$\gamma_{\text{SC}} = K\left[1+\sqrt{\frac{\bar{b}_2}{K}}Q^{-1}\left(1-\sqrt[M]{1-P_{\text{FA}}}\right)\right]. \tag{24}$$

On the other hand, the probability of detection cannot be expressed in closed form, although it can be straightforwardly computed by means of a Gaussian integration routine; see Appendix B. It must be noted that, in contrast with GED, the performance of the SC detector does depend on the spherical component $\bar{\boldsymbol{h}}$.

C. Equal Gain Combining detector

For EGC detection, an estimate of the phases $\{\theta_i\}_{i=1}^M$ introduced at the different branches is needed in order to combine the respective signals as per (16). Considering again the low SNR approximation (18), it is seen that in order to obtain the ML estimates we must maximize the following quantity w.r.t. $\theta_1, \ldots, \theta_M$:

$$\boldsymbol{r}^H\mathcal{G}\boldsymbol{r} = \sum_{n=1}^{M}\sum_{m=1}^{M}|h_n||h_m|\boldsymbol{r}_n^H\boldsymbol{C}\boldsymbol{r}_m\mathrm{e}^{-\jmath(\theta_m-\theta_n)}. \tag{25}$$

Let $a_{nm} \doteq |h_n||h_m|\boldsymbol{r}_n^H \boldsymbol{C}\boldsymbol{r}_m$. Since $a_{nm} = a_{mn}^*$, it is clear that

$$\begin{aligned} \boldsymbol{r}^H \mathcal{G} \boldsymbol{r} &= \sum_{m=1}^{M} a_{mm} + 2\sum_{n=1}^{M}\sum_{m=n+1}^{M} \mathrm{Re}\{a_{nm} \mathrm{e}^{-\jmath(\theta_m - \theta_n)}\} \\ &\leq \sum_{m=1}^{M} a_{mm} + 2\sum_{n=1}^{M}\sum_{m=n+1}^{M} |a_{nm}|, \end{aligned} \tag{26}$$

with equality iff $\theta_m - \theta_n = \arg\{a_{nm}\}$ for all (n, m) such that $m > n$. These constitute a set of $M(M-1)/2$ (linear) conditions on our M free parameters, which in general cannot be satisfied if $M > 3$. Nevertheless, careful inspection of the resulting detection statistic $\boldsymbol{s}^H \boldsymbol{C}\boldsymbol{s}$ with $\boldsymbol{s} = \sum_{l=1}^{M} \mathrm{e}^{-\jmath\hat{\theta}_l}\boldsymbol{r}_l$ reveals that it is a function of the phase differences $\hat{\theta}_{mn} \doteq \hat{\theta}_m - \hat{\theta}_n$ only. Thus, if we take these phase differences as our free optimization variables and neglect the dependence among them, the corresponding ML estimates become $\hat{\theta}_{mn} = \arg\{\boldsymbol{r}_n^H \boldsymbol{C}\boldsymbol{r}_m\}$. This yields the following EGC detection rule:

$$T_{\text{EGC}} \doteq \sum_{n=1}^{M}\sum_{m=1}^{M} |\boldsymbol{r}_m^H \boldsymbol{C}\boldsymbol{r}_n| \underset{\mathcal{H}_0}{\overset{\mathcal{H}_1}{\gtrless}} \gamma_{\text{EGC}}, \tag{27}$$

i.e., the lack of knowledge about the phase differences is sidestepped by considering the *modulus* of the crosscorrelation terms.

Unfortunately, finding the distribution of T_{EGC} (under either hypothesis) is intractable. An asymptotic Gaussian approximation is used in Appendix C, showing that for large K, the threshold γ_{EGC} for a given false alarm rate P_{FA} can be obtained as

$$\gamma_{\text{EGC}} = KM\left[1 + \frac{M-1}{2}\sqrt{\frac{\pi\bar{b}_2}{K}} + \sqrt{\frac{\bar{b}_2}{2KM}[(\pi-2) + M(4-\pi)}Q^{-1}(P_{\text{FA}})\right]. \tag{28}$$

For large K, the probability of detection is given by

$$P_{\text{D}}^{\text{EGC}} \approx Q\left(\frac{\sqrt{\frac{\pi-2}{2M} + 2 - \frac{\pi}{2}}Q^{-1}(P_{\text{FA}}) + \frac{M-1}{2}\sqrt{\pi} - \sqrt{K\bar{b}_2}\kappa\rho}{\sqrt{\frac{\bar{b}_4}{\bar{b}_2}\kappa^2\rho^2 + 2\frac{\bar{b}_3}{\bar{b}_2}\kappa\rho + 1}}\right), \tag{29}$$

where $\kappa \doteq \|\boldsymbol{h}\|_1^2/\|\boldsymbol{h}\|_2^2 = \|\bar{\boldsymbol{h}}\|_1^2$. Note that (29) is a function of the *scaled* average SNR per antenna $\kappa\rho$, and that the scaling term $\kappa \in [1, M]$ achieves its maximum value when all elements of $\boldsymbol{h}$ have the same magnitude. This is intuitively satisfying, since it is precisely in such scenarios that one expects the EGC detector to perform best.

D. Maximal Ratio Combining detector

For MRC detection, an estimate of the spherical component $\bar{\boldsymbol{h}} = \boldsymbol{h}/\|\boldsymbol{h}\|_2$ is needed. Let us introduce the data matrix $\boldsymbol{R} \doteq [\,\boldsymbol{r}_1 \cdots \boldsymbol{r}_M\,]$. Focusing again on the low SNR approximation (18), the ML estimate of $\bar{\boldsymbol{h}}$ must maximize

$$\begin{aligned} \boldsymbol{r}^H \mathcal{G} \boldsymbol{r} &= \boldsymbol{r}^H(\boldsymbol{h}\boldsymbol{h}^H \otimes \boldsymbol{C})\boldsymbol{r} \\ &= \boldsymbol{h}^H(\boldsymbol{R}^H \boldsymbol{C}\boldsymbol{R})^*\boldsymbol{h} \\ &= \|\boldsymbol{h}\|_2^2 \bar{\boldsymbol{h}}^H(\boldsymbol{R}^H \boldsymbol{C}\boldsymbol{R})^*\bar{\boldsymbol{h}}. \end{aligned} \tag{30}$$

This is achieved when $\bar{\boldsymbol{h}}$ is the unit-norm eigenvector of $(\boldsymbol{R}^H\boldsymbol{C}\boldsymbol{R})^*$ associated to its largest eigenvalue (up to a phase term $\mathrm{e}^{j\phi}$ which does not affect the test). This results in the following MRC detection rule:

$$T_{\text{MRC}} \doteq \lambda_{\max}(\boldsymbol{R}^H\boldsymbol{C}\boldsymbol{R}) \underset{\mathcal{H}_0}{\overset{\mathcal{H}_1}{\gtrless}} \gamma_{\text{MRC}}. \tag{31}$$

Note that neither T_{EGC} nor T_{MRC} lend themselves to distributed implementation, since they require the computation of (spectrally weighted) crosscorrelations across the different antennas.

In order to obtain the performance of the MRC detector, the distribution of the largest eigenvalue of the random matrix $\boldsymbol{R}^H\boldsymbol{C}\boldsymbol{R}$ under each hypothesis has to be found. For a general positive semidefinite Toeplitz $\boldsymbol{C}$, this remains an open problem. In Appendix D we consider a particular case, namely a covariance matrix corresponding to a strictly bandlimited signal with flat psd within its passband, and with normalized spectral support $B \in (0, 1]$. In that case, under $\mathcal{H}_0$ the statistic T_{MRC} asymptotically becomes a (linear transformation of) a Tracy-Widom random variable, whereas under $\mathcal{H}_1$ it follows a Gaussian distribution that is independent of the spherical component $\bar{\boldsymbol{h}}$. These results are asymptotic in both K and M and need not be accurate for moderate values of these parameters. However, they do capture the correct trends with system parameters, as shown in the next section.

V. Numerical results

We proceed to examine the performance of the proposed detectors, using the analytical results derived in the Appendix together with Monte Carlo simulations.

A. Statistical distributions

In order to validate the approximations used in the derivation of the analytical results, in Fig. 1 the theoretical and empirical distributions (histograms) of the test statistics in two different scenarios are shown.

- *Scenario 1:* $K = 1024$ samples per antenna, $M = 2$ antennas with the same SNR (-11 dB). In this experiment we used I/Q samples from a multicarrier baseband signal adhering to the digital TV DVB-T standard [23]. The psd of this signal is approximately flat within the baseband bandwidth ($7.61/2$ MHz). Sampling was asynchronous, and at a rate $f_s = 8$ Msps (which is the RF channel separation). Hence, the multicarrier signal occupies a fraction $B \approx 97\%$ of the Nyquist bandwidth. Note that this class of signal fits well the assumptions in the derivations of Appendix D. As seen in Fig. 1(a)-(d), the analytical distributions of the four detectors considered fit quite well the empirical histograms.
- *Scenario 2:* $K = 512$ samples per antenna, $M = 4$ antennas with different SNR (-7, -12, -14 and -18 dB). In this case, the primary signal is a 16-QAM baseband signal with square-root raised cosine (SRRC) pulse shaping and roll-off factor 0.5. I/Q samples were taken asynchronously at the Nyquist rate $f_s = 1.5R_s$, where R_s is the baud rate. Note that the psd of this SRRC-shaped signal does not strictly conform to the "flat within the passband" assumption used in Appendix D to derive the analytical distribution of the MRC statistic; hence, we have regarded this psd as constant within $|f| \leq R_s/2$ and zero elsewhere in order to obtain an approximate MRC distribution.

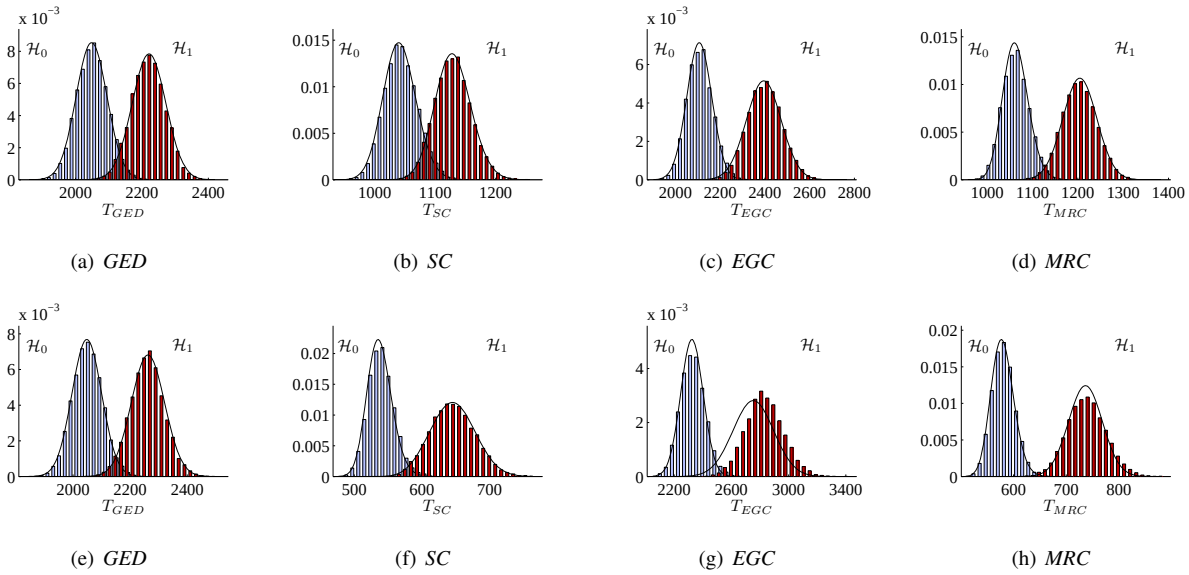

(a) *GED* (b) *SC* (c) *EGC* (d) *MRC*

(e) *GED* (f) *SC* (g) *EGC* (h) *MRC*

Fig. 1. Theoretical and empirical distributions of the detectors: $M = 2$, $K = 1024$, multicarrier signal (a)-(d); $M = 4$, $K = 512$, SRRC with 50% excess bandwidth (e)-(h).

In Fig. 1(e)-(h) it is seen that the analytical distributions obtained under $\mathcal{H}_0$ closely match the empirical histograms for the four detectors. On the other hand, under $\mathcal{H}_1$ we observe some deviation between analytical and theoretical results for the EGC and MRC detectors. In the case of the MRC test, this deviation is not too pronounced and is likely to be due to the approximations discussed above. Regarding the EGC detector, we must recall that the analytical distribution proposed (Gaussian approximation) is asymptotic in K. A close look at the analysis in Appendix C shows that in order to achieve a certain degree of accuracy the value of K must increase if the SNR at any of the antennas is very low, as is the case in this example.

B. Effect of the number of antennas

In order to show the effect of the number of antennas on the proposed detectors, the complementary Receiver Operation Characteristic (ROC) curves of a system with $M = 2$ antennas are compared to those of another with $M = 4$, for a constant total number of samples $MK = 2^{11}$. The same multicarrier signal and sampling rate of Scenario 1 from the previous section are considered.

Fig. 2 shows the analytical and empirical ROC curves for the four schemes in both settings with the SNR at each of the antennas fixed to -10 dB. The GED curves are almost identical in both settings, due to the fact that, from (22), GED performance depends only on the total number of samples MK in the low SNR regime. The performance of the SC detector in this setting actually deteriorates if the number of antennas is increased. On the other hand, both EGC and MRC detection schemes improve with increasing M. The fact that EGC may perform even better than MRC in Fig. 2 is due to the uniform instantaneous SNR per antenna distribution used in this setting, which better fits the simplifying assumptions in the derivation of the EGC test. Again, for $M = 4$ a noticeable mismatch

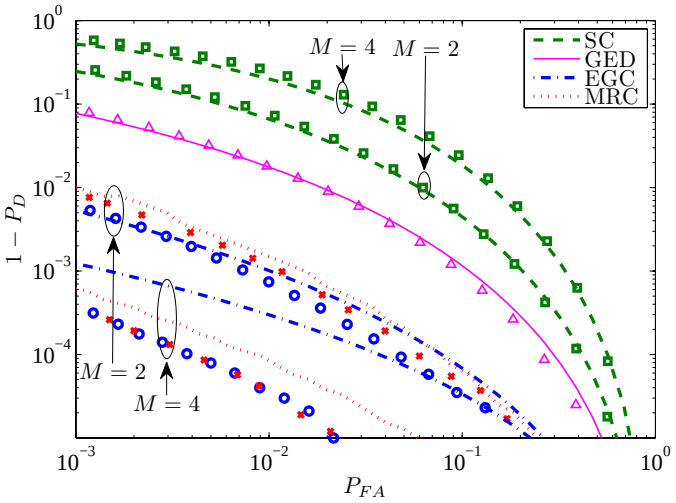

Fig. 2. ROC curves with $M = 2$ and 4 antennas for $\rho = -10$ dB and uniform distribution of instantaneous SNR across antennas ($\kappa = M$).

between the analytical and empirical EGC curves appears, due to the limitations of the asymptotic approximations employed.

C. Effect of SNR distribution across antennas

We now assess the effect of a non-uniform distribution of the instantaneous SNR across the antennas, quantified by the parameter $\kappa = \|\bar{\boldsymbol{h}}\|_1^2$. We considered $M = 4$ antennas, $K = 512$ samples per antenna, average SNR per antenna $\rho = -5$ dB, and a multicarrier signal in the same scenario as in the previous examples. Fig. 3 shows the probability of missed detection as a function of κ (using $\bar{\boldsymbol{h}} = [\, h \; h \; h \; \sqrt{1-3h^2}\,]^T$ with $h \in [0, \frac{1}{2}]$) for a fixed false alarm rate $P_{\text{FA}} = 0.05$. As expected from the analysis, the performances of GED and MRC detectors are independent of the spherical component $\bar{\boldsymbol{h}}$. Whereas EGC performs better with an uniform SNR distribution ($\kappa = M$), the reverse is true for the SC detector, which benefits from concentration of the SNR at a single antenna ($\kappa \to 1$). This is in agreement with the respective models under which these detectors constitute approximate GLR tests. In this sense, it is interesting to compare the performance of EGC and SC to that of MRC, which is the GLR test when no structure on $\boldsymbol{h}$ is assumed. SC clearly outperforms MRC when κ becomes small, and this is intuitively satisfying since the data model is more efficiently exploited. On the other hand, the performance of EGC turns out to be no better than that of MRC, even as $\kappa \to M$. Finally, note that the asymptotic analytical results, while inaccurate at some points due to the small number of samples, show the right global behavior.

D. Detection in fading environments

Up to this point the instantaneous SNR at each antenna has been fixed during the execution of a given experiment. Now we investigate the performance of the proposed detectors with Ricean fading, accounting for a deterministic

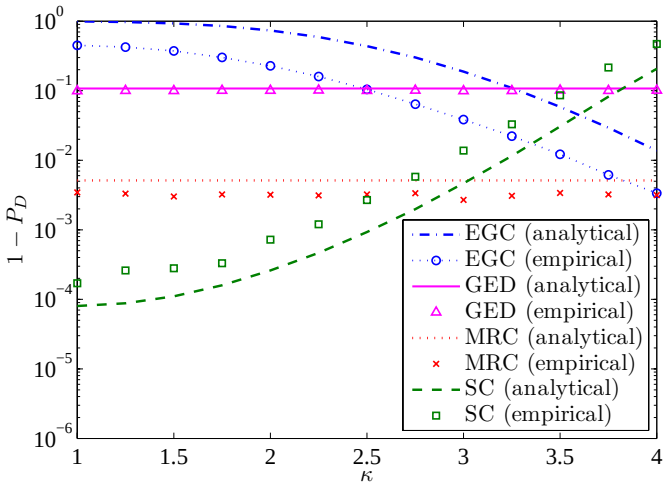

Fig. 3. Probability of miss vs. κ for $M = 4$, $K = 512$, $\rho = -5$ dB and $P_{\text{FA}} = 0.05$.

line-of-sight (LOS) component that illuminates the array uniformly, as well as non-line-of-sight (NLOS) spatially uncorrelated random scattering:

$$\boldsymbol{h} = \sqrt{\bar{\rho}} \left(\sqrt{\frac{K_R}{1+K_R}} \boldsymbol{h}_{\text{LOS}} + \sqrt{\frac{1}{1+K_R}} \boldsymbol{h}_{\text{NLOS}} \right), \tag{32}$$

where K_R is the Rice factor (ratio of deterministic-to-scattered power), $\boldsymbol{h}_{\text{NLOS}}$ is zero-mean circular complex Gaussian with $E\{\boldsymbol{h}_{\text{NLOS}} \boldsymbol{h}_{\text{NLOS}}^H\} = \boldsymbol{I}_M$, and $\boldsymbol{h}_{\text{LOS}} = [\, 1 \; \mathrm{e}^{\jmath\phi} \; \cdots \; \mathrm{e}^{\jmath(M-1)\phi} \,]^T$ the response of a uniform linear array. The relative phase ϕ between adjacent antennas is modeled as a random variable uniformly distributed in $[0, \pi]$ and independent of $\boldsymbol{h}_{\text{NLOS}}$. The mean SNR per antenna is $\bar{\rho} = E\{\|\boldsymbol{h}\|^2\}/M$.

Fig. 4 shows the results in terms of missed detection probability vs. $\bar{\rho}$, for a setting with $M = 4$, $K = 256$, with multicarrier signals occupying $B \approx 97\%$ of the Nyquist bandwidth, and fixing $P_{\text{FA}} = 0.05$. Two cases are shown: $K_R = 0$ (Rayleigh fading, i.e. no LOS component), and $K_R = 10$ (LOS power 10 dB above scattered power). It is seen that the asymptotic slope of the curves is the same for all detectors and depends only on K_R, and that the MRC detector consistently outperforms the other three schemes. However, the performance loss of the EGC detector is quite small: less than 0.5 dB with Rayleigh fading, and almost negligible for $K_R = 10$. This makes the EGC detector appealing in order to avoid the eigenvalue computations that MRC requires.

E. Exploiting a priori *information about spectral shape*

To close this section we illustrate the benefits of exploiting the knowledge about the spectral shape of the primary signal. To this end we consider the detection of a Gaussian Minimum Shift Keying (GMSK) waveform synthesized according to the GSM cellular standard, downconverted to baseband and I/Q-sampled at $f_s = 600$ Ksps. Rayleigh fading is assumed, and the number of antennas is $M = 4$. We picked $K = 256$ samples per antenna and fixed $P_{\text{FA}} = 0.05$.

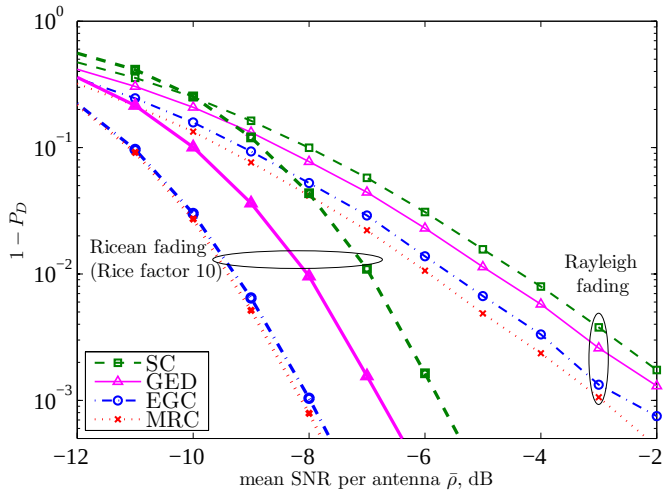

Fig. 4. Probability of miss vs. mean SNR with channel fading for $M = 4$, $K = 256$, and $P_{\text{FA}} = 0.05$ (multicarrier signal).

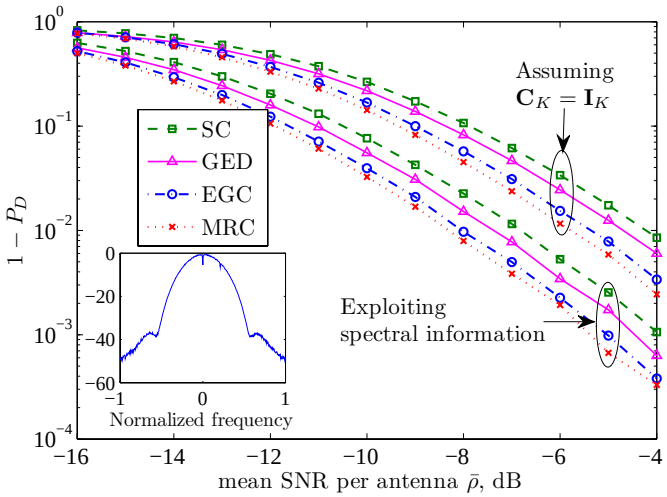

Fig. 5. Probability of miss vs. mean SNR with Rayleigh fading for $M = 4$, $K = 256$, and $P_{\text{FA}} = 0.05$ (GMSK signal, with psd shown in inset).

In Fig. 5 the performance of the proposed detectors is compared to that of the analogous schemes but using $\boldsymbol{C} = \boldsymbol{I}_K$, i.e. neglecting *a priori* knowledge. This has the advantage of disposing of the FFT operations at each antenna, reducing the computational cost of the detectors. However, the performance loss incurred is significant (larger than 2 dB in this example). This is explained by the fact that only spatial correlation and total power are exploited by these simplified detectors, but not the *temporal* correlation properties of the signal.

VI. Conclusions

We have considered the problem of multiantenna detection exploiting *a priori* knowledge of the power spectral density of the signal. In this way, signal correlation is jointly exploited in both temporal and spatial domains. The low SNR approximation allows the derivation of GLR tests closely related to well-known diversity combining schemes. Using the asymptotic diagonalization of Toeplitz matrices, the test statistics can be efficiently computed using FFT techniques. Among the proposed schemes, the MRC detector is optimal and does not depend on the spatial distributions of the unknown channel gains. Nevertheless, in fading scenarios the loss incurred by the EGC test is small, and thus this detector provides a good tradeoff between complexity and performance.

References

[1] R. López-Valcarce, G. Vazquez-Vilar, and M. Alvarez-Díaz, "Multiantenna detection of multicarrier primary signals exploiting spectral a priori information," in *Proc. Int. Conf. Cognitive Radio Oriented Wireless Networks and Comm. (CROWNCOM)*, Jun. 2009.

[2] I. Akyildiz, W.-Y. Lee, M. Vuran, and S. Mohanty, "A survey on spectrum management in cognitive radio networks," *IEEE Commun. Mag.*, vol. 46, no. 4, pp. 40–48, April 2008.

[3] J. M. Peha, "Sharing spectrum through spectrum policy reform and cognitive radio," *Proc. IEEE*, vol. 97, no. 4, pp. 708–719, Apr 2009.

[4] G. Ganesan and Y. Li, "Cooperative spectrum sensing in cognitive radio, part I: Two user networks," *IEEE Trans. Wireless Commun.*, vol. 6, no. 6, pp. 2204–2213, Jun. 2007.

[5] ——, "Cooperative spectrum sensing in cognitive radio, part II: Multiuser networks," *IEEE Trans. Wireless Commun.*, vol. 6, no. 6, pp. 2214–2222, Jun. 2007.

[6] A. V. Dandawaté and G. B. Giannakis, "Statistical tests for presence of cyclostationarity," *IEEE Trans. Signal Process.*, vol. 42, no. 9, pp. 2355–2359, Sep. 1994.

[7] M. Oner and F. Jondral, "On the extraction of the channel allocation information in spectrum pooling systems," *IEEE J. Sel. Areas Commun.*, vol. 25, no. 3, pp. 558–565, Apr. 2007.

[8] S. Chaudhari, V. Koivunen, and H. Poor, "Autocorrelation-based decentralized sequential detection of ofdm signals in cognitive radios," *IEEE Trans. Signal Process.*, vol. 57, no. 7, pp. 2690–2700, Jul. 2009.

[9] M. Derakhtian, A. Tadaion, S. Gazor, and M. Nayebi, "Invariant activity detection of a constant magnitude signal with unknown parameters in white Gaussian noise," *IET Commun.*, vol. 3, no. 8, pp. 1420–1431, Aug. 2009.

[10] A. Perez-Neira, M. Lagunas, M. Rojas, and P. Stoica, "Correlation matching approach for spectrum sensing in open spectrum communications," *IEEE Trans. Signal Process.*, vol. 57, no. 12, pp. 4823–4836, Dec. 2009.

[11] M. Derakhtian, A. Tadaion, and S. Gazor, "Detection of a bandlimited signal with unknown parameters," in *IEEE/SP Work. Stat. Signal Process. (SSP)*, Aug. 2009, pp. 145–148.

[12] Y. Zeng and Y.-C. Liang, "Spectrum-sensing algorithms for cognitive radio based on statistical covariances," *IEEE Trans. Veh. Technol.*, vol. 58, no. 4, pp. 1804–1815, May 2009.

[13] Z. Quan, W. Zhang, S. J. Shellhammer, and A. H. Sayed, "Optimal spectral feature detection for spectrum sensing at very low SNR," *IEEE Trans. Commun.*, vol. 59, no. 1, pp. 201–212, Jan. 2011.

[14] H. Urkowitz, "Energy detection of unknown deterministic signals," *Proc. IEEE*, vol. 55, no. 4, pp. 523–531, April 1967.

[15] D. Cabric, "Addressing the feasibility of cognitive radios," *IEEE Signal Process. Mag.*, vol. 25, no. 6, pp. 85–93, Nov. 2008.

[16] A. Taherpour, M. Nasiri-Kenari, and S. Gazor, "Multiple antenna spectrum sensing in cognitive radios," *IEEE Trans. Wireless Commun.*, vol. 9, no. 2, pp. 814–823, Feb. 2010.

[17] R. Zhang, T. Lim, Y.-C. Liang, and Y. Zeng, "Multi-antenna based spectrum sensing for cognitive radios: A GLRT approach," *IEEE Trans. Commun.*, vol. 58, no. 1, pp. 84–88, Jan. 2010.

[18] P. Wang, J. Fang, N. Han, and H. Li, "Multiantenna-assisted spectrum sensing for cognitive radio," *IEEE Trans. Veh. Technol.*, vol. 59, pp. 1791–1800, 2010.

[19] W. Zhang, H. Poor, and Z. Quan, "Frequency-domain correlation: an asymptotically optimum approximation of quadratic likelihood ratio detectors," *IEEE Trans. Signal Process.*, vol. 58, no. 3, pp. 969–979, Mar. 2010.

[20] S. M. Kay, *Fundamentals of statistical signal processing: detection theory*. Englewood Cliffs, NJ: Prentice-Hall, 1998.

[21] M. K. Simon and M.-S. Alouini, *Digital communication over fading channels*. Hoboken, NJ: Wiley-Interscience, John Wiley and Sons, 2004.

[22] R. M. Gray, *Toeplitz and circulant matrices: a review*. New York: Hanover/Now, 2006.

[23] EN 300 744 V1.5.1, *Digital Video Broadcasting (DVB); Framing structure, channel coding and modulation for terrestrial television*. ETSI, Nov. 2004.

[24] B. Porat and B. Friedlander, "Computation of the exact information matrix of Gaussian time series with stationary random components," *IEEE Trans. Acoust., Speech, Signal Process.*, vol. 34, no. 1, pp. 118 – 130, Feb. 1986.

[25] J. Hayya, D. Armstrong, and N. Gressis, "A Note on the Ratio of Two Normally Distributed Variables," *Management Science*, vol. 21, no. 11, pp. 1338–1341, Jul. 1975.

[26] A. M. Tulino and S. Verdú, "Random matrix theory and wireless communications," *Commun. Inf. Theory*, vol. 1, pp. 1–182, June 2004. [Online]. Available: http://portal.acm.org/citation.cfm?id=1166373.1166374

[27] N. E. Karoui, "Recent results about the largest eigenvalue of random covariance matrices and statistical application," *Acta Physica Polonica B*, vol. 36, no. 9, pp. 2681–2697, Sep. 2005.

[28] J. Baik and J. W. Silverstein, "Eigenvalues of large sample covariance matrices of spiked population models," *J. Multivar. Anal.*, vol. 97, pp. 1382–1408, Jul. 2006. [Online]. Available: http://portal.acm.org/citation.cfm?id=1150619.1150629

APPENDIX
STATISTICAL ANALYSIS FOR LARGE DATA RECORDS

Let $t_{ij} \doteq \boldsymbol{r}_i^H \boldsymbol{C} \boldsymbol{r}_j \mathrm{e}^{\jmath\theta_{ij}}$ denote the phase-aligned spectrally weighted crosscorrelation between antennas i and j, where $\theta_{ij} \doteq \arg\{h_i\} - \arg\{h_j\}$. For large K, we can invoke the central limit theorem and assume that t_{ij} is Gaussian distributed. Under this approximation, and using the fact that for zero-mean complex circular Gaussian vectors $\boldsymbol{x}$, $\boldsymbol{y}$, $\boldsymbol{u}$, $\boldsymbol{v}$, and constant $\boldsymbol{A}$, $\boldsymbol{B}$, it holds that

$$\mathrm{E}\{(\boldsymbol{x}^H\boldsymbol{A}\boldsymbol{y})(\boldsymbol{u}^H\boldsymbol{B}\boldsymbol{v})\} = \mathrm{tr}\left[\boldsymbol{A}\mathrm{E}\{\boldsymbol{y}\boldsymbol{x}^H\}\right]\mathrm{tr}\left[\boldsymbol{B}\mathrm{E}\{\boldsymbol{v}\boldsymbol{u}^H\}\right] + \mathrm{tr}\left[\boldsymbol{A}\mathrm{E}\{\boldsymbol{y}\boldsymbol{u}^H\}\boldsymbol{B}\mathrm{E}\{\boldsymbol{v}\boldsymbol{x}^H\}\right], \tag{33}$$

(see e.g. [24]), then one finds that

$$\begin{aligned}
\mathrm{E}\{t_{ij}\} &= K(|h_i||h_j|\bar{b}_2 + \delta_{ij}), && (34)\\
\mathrm{var}\{t_{ij}\} &= K\left[|h_i|^2|h_j|^2\bar{b}_4 + (|h_i|^2 + |h_j|^2)\bar{b}_3 + \bar{b}_2\right], && (35)\\
\mathrm{E}\{t_{ij}^2\} - \mathrm{E}^2\{t_{ij}\} &= K\left[|h_i|^2|h_j|^2\bar{b}_4 + (2|h_i||h_j|\bar{b}_3 + \bar{b}_2)\delta_{ij}\right], && (36)\\
\mathrm{E}\{t_{ij}t_{kl}^*\} - \mathrm{E}\{t_{ij}\}\mathrm{E}\{t_{kl}^*\} &= K\left[|h_i||h_j||h_k||h_l|\bar{b}_4 + (|h_j||h_l|\delta_{ik} + |h_i||h_k|\delta_{jl})\bar{b}_3 + \bar{b}_2\delta_{ik}\delta_{jl}\right]. && (37)
\end{aligned}$$

From (34)-(36), it follows that for $i \neq j$ the real and imaginary parts of t_{ij} are uncorrelated ($\mathrm{E}\{\Re\{t_{ij}\}\Im\{t_{ij}\}\} - \mathrm{E}\{\Re\{t_{ij}\}\}\mathrm{E}\{\Im\{t_{ij}\}\} = 0$), with variances given by

$$\begin{aligned}
\mathrm{var}\{\Re\{t_{ij}\}\} &= K\left[|h_i|^2|h_j|^2\bar{b}_4 + \frac{1}{2}\left((|h_i|^2 + |h_j|^2)\bar{b}_3 + \bar{b}_2\right)\right], && (38)\\
\mathrm{var}\{\Im\{t_{ij}\}\} &= \frac{K}{2}\left[(|h_i|^2 + |h_j|^2)\bar{b}_3 + \bar{b}_2\right]. && (39)
\end{aligned}$$

A. Generalized Energy Detector

The GED statistic can be written as $T_{\text{GED}} = \mathbf{1}^T \boldsymbol{t}$, where $\boldsymbol{t} \doteq [\, t_{11} \cdots t_{MM} \,]^T$. For large K, $\boldsymbol{t}$ is normally distributed; from (34)-(35), its mean and covariance are

$$\mathrm{E}\{\boldsymbol{t}\} = K\left(\bar{b}_2 \boldsymbol{g} + \mathbf{1}\right), \tag{40}$$

$$\mathrm{cov}\{\boldsymbol{t}, \boldsymbol{t}\} = K\left(\bar{b}_4 \boldsymbol{g}\boldsymbol{g}^H + \bar{b}_2 \boldsymbol{I} + 2\bar{b}_3 \,\mathrm{diag}\{\boldsymbol{g}\}\right), \tag{41}$$

where $\boldsymbol{g} \doteq [\, |h_1|^2 \; |h_2|^2 \; \cdots \; |h_M|^2 \,]^T$. Thus, T_{GED} is asymptotically Gaussian; Using (40)-(41), its mean and variance are found to be

$$\mu_{\text{GED}}(\|\boldsymbol{h}\|_2) \doteq E\{T_{\text{GED}}\} = K\left(\|\boldsymbol{h}\|_2^2 \bar{b}_2 + M\right), \tag{42}$$

$$\alpha^2_{\text{GED}}(\|\boldsymbol{h}\|_2) \doteq \mathrm{var}\{T_{\text{GED}}\} = K\left(\|\boldsymbol{h}\|_2^4 \bar{b}_4 + 2\|\boldsymbol{h}\|_2^2 \bar{b}_3 + M\bar{b}_2\right). \tag{43}$$

Therefore, for a given threshold γ_{GED} the probabilities of false alarm and detection are respectively given by

$$P_{\text{FA}}^{\text{GED}} = Q\left(\frac{\gamma_{\text{GED}} - \mu_{\text{GED}}(0)}{\alpha_{\text{GED}}(0)}\right), \tag{44}$$

$$P_{\text{D}}^{\text{GED}} = Q\left(\frac{\gamma_{\text{GED}} - \mu_{\text{GED}}(\|\boldsymbol{h}\|_2)}{\alpha_{\text{GED}}(\|\boldsymbol{h}\|_2)}\right), \tag{45}$$

from which (21)-(22) follow.

B. Selection Combining Detector

The statistic of the SC detector is $T_1 = \max_{1 \le i \le M} t_{ii}$. For a given threshold γ_{SC}, and M antennas, the false alarm probability is

$$P_{\text{FA}}^{\text{SC}}(M) = 1 - \Pr\left\{t_{ii} \le \gamma_{\text{SC}},\, 1 \le i \le M \mid \mathcal{H}_0\right\} \tag{46}$$

$$= 1 - \prod_{i=1}^{M} \Pr\left\{t_{ii} \le \gamma_{\text{SC}} \mid \mathcal{H}_0\right\} \tag{47}$$

$$= 1 - [1 - P_{\text{FA}}(1)]^M, \tag{48}$$

where we have used the fact that under $\mathcal{H}_0$ the t_{ii} are independent, and $P_{\text{FA}}(1)$ denotes the False Alarm probability of a single-antenna detector with the same threshold γ_{SC}, which is found from (44):

$$P_{\text{FA}}(1) = Q\left(\frac{\gamma_{\text{SC}} - K}{\sqrt{\bar{b}_2 K}}\right), \tag{49}$$

from which (24) follows. On the other hand, the probability of detection is

$$P_{\text{D}}^{\text{SC}}(M) = 1 - \Pr\left\{t_{ii} \le \gamma_{\text{SC}},\, 1 \le i \le M \mid \mathcal{H}_1\right\}. \tag{50}$$

Since the random variables t_{ii} are not independent under $\mathcal{H}_1$, (50) does not factor out as in (47) in general (except if all but one of the channel coefficients are zero, in which case the covariance matrix (41) becomes diagonal). Thus, the computation of (50) involves the integration of a multivariate Gaussian with mean and covariance given by (40)-(41). This can be done numerically using e.g. Matlab's `mvncdf` Gaussian integration package.

C. Equal Gain Combining detector

The statistic of the EGC detector can be rewritten as

$$T_{\text{EGC}} = \sum_{i=1}^{M}\sum_{j=1}^{M} |t_{ij}|. \tag{51}$$

Note that $|t_{ii}| = t_{ii}$, $1 \le i \le M$, which is Gaussian distributed for large K under both hypotheses. On the other hand, for $i \neq j$, t_{ij} is complex-valued Gaussian with independent real and imaginary parts.

1) Distribution of T_{EGC} under $\mathcal{H}_0$: If $h_i = h_j = 0$, then the real and imaginary parts of t_{ij}, $i \neq j$, have both zero mean and the same variance. Therefore $|t_{ij}|$ is Rayleigh distributed with

$$E\{|t_{ij}|\,|\,\mathcal{H}_0\} = \frac{1}{2}\sqrt{K\pi\bar{b}_2}, \tag{52}$$

$$\text{var}\{|t_{ij}|\,|\,\mathcal{H}_0\} = K\left(1-\frac{\pi}{4}\right)\bar{b}_2, \tag{53}$$

for $i \neq j$. Note from (37) that if $(i,j) \neq (k,l)$ then t_{ij} and t_{kl} are uncorrelated (and hence independent for large K) under $\mathcal{H}_\prime$, and therefore the different terms $|t_{ij}|$ in (51) become independent as well. Thus T_{EGC} is the sum of M Gaussian- and $M(M-1)/2$ (since $|t_{ij}| = |t_{ji}|$) Rayleigh-distributed, independent random variables. There is no simple closed-form expression for the resulting distribution; we propose a Gaussian approximation, based on the asymptotic mean and variance given by

$$E\{T_{\text{EGC}}\} = \sum_{i=1}^{M} K + \sum_{i=1}^{M}\sum_{j=1,j\neq i}^{M} \frac{1}{2}\sqrt{\pi K\bar{b}_2} \tag{54}$$

$$= KM\left(1 + \frac{M-1}{2}\sqrt{\frac{\pi\bar{b}_2}{K}}\right), \tag{55}$$

$$\text{var}\{T_{\text{EGC}}\} = \sum_{m=1}^{M}\text{var}\{|t_{mm}|\} + \sum_{m=1}^{M}\sum_{i=1,i>m}^{M}\text{var}\{2|t_{mi}|\} \tag{56}$$

$$= \sum_{m=1}^{M} K\bar{b}_2 + \sum_{m=1}^{M}\sum_{i=1,i>m}^{M} 4K(1-\frac{\pi}{4})\bar{b}_2 \tag{57}$$

$$= KM\left(\left(\frac{\pi}{2}-1\right) + M\left(2-\frac{\pi}{2}\right)\right)\bar{b}_2, \tag{58}$$

from which (28) follows.

2) Distribution of T_{EGC} under $\mathcal{H}_1$: For $i \neq j$, t_{ij} asymptotically follows a complex normal distribution centered on the real axis; its real and imaginary parts are uncorrelated and have different variances in general. We can write

$$|t_{ij}| = |\Re\{t_{ij}\}|\sqrt{1+z_{ij}^2}, \tag{59}$$

where $z_{ij} \doteq \Im\{t_{ij}\}/\Re\{t_{ij}\}$. Note that z_{ij} is the ratio of two uncorrelated Gaussian random variables, and there is no closed-form expression for its distribution. However, from [25], if the coefficient of variation of the denominator (defined as the ratio of its standard deviation to its mean value) is less than 0.39, there exist a transformation $g(\cdot)$ such that the distribution of $g(z_{ij})$ can be accurately approximated by a standard Gaussian $\mathcal{N}(0,1)$. In our case,

the coefficient of variation is

$$\beta_{ij} \doteq \frac{\sqrt{\mathrm{var}\{\Re\{t_{ij}\}\}}}{E\{\Re\{t_{ij}\}\}} = \frac{1}{K}\frac{\sqrt{|h_i|^2|h_j|^2\bar{b}_4 + \frac{1}{2}\left((|h_i|^2+|h_j|^2)\bar{b}_3+\bar{b}_2\right)}}{|h_i||h_j|\bar{b}_2}. \tag{60}$$

Provided that $h_i \neq 0$, $h_j \neq 0$, then (60) goes to zero as $K \to \infty$. Thus, for large enough K, the random variable

$$g(z_{ij}) \doteq \frac{\mathrm{E}\{\Re\{t_{ij}\}\}z_{ij} - E\{\Im\{t_{ij}\}\}}{\sqrt{\mathrm{var}\{\Re\{t_{ij}\}\}z_{ij}^2 + \mathrm{var}\{\Im\{t_{ij}\}\}}} \tag{61}$$

$$= \sqrt{K}\frac{|h_i||h_j|\bar{b}_2 z_{ij}}{\sqrt{\|h_i|^2|h_j|^2\bar{b}_4 z_{ij}^2 + \frac{1}{2}\left((|h_i|^2+|h_j|^2)\bar{b}_3+\bar{b}_2\right)(1+z_{ij}^2)}} \tag{62}$$

is approximately zero-mean Gaussian with unit variance [25]. Since the transformation $g(z)$ in (62) is one-to-one, it follows that

$$\Pr\{z_{ij}^2 > \epsilon\} = 2Q(g(\sqrt{\epsilon})), \tag{63}$$

which approaches zero exponentially fast as $K \to \infty$. Therefore, for K large enough, it is reasonable to approximate $|t_{ij}| \approx |\Re\{t_{ij}\}|$ in (59). Moreover, with β_{ij} as in (60), one has $\Pr\{\Re\{t_{ij}\} < 0\} = Q(\beta_{ij}^{-1})$, which also goes to zero exponentially with K.

In view of all these, if $|h_m| > 0$ for $m = 1, \ldots, M$ then for sufficiently large K the terms $|t_{ij}|$, $i \neq j$, behave as correlated real-valued Gaussian random variables. Thus T_{EGC} becomes approximately Gaussian, with expected value

$$E\{T_{\text{EGC}}\} \approx \sum_{i=1}^{M}\sum_{j=1}^{M} E\{\Re\{t_{ij}\}\} = K\left(\|\boldsymbol{h}\|_1^2\bar{b}_2 + M\right) \tag{64}$$

and variance

$$\mathrm{var}\{T_{\text{EGC}}\} \approx \sum_{i,j,k,l}\left[E\{\Re\{t_{ij}\}\Re\{t_{kl}\}\} - E\{\Re\{t_{ij}\}\}E\{\Re\{t_{kl}\}\}\right] \tag{65}$$

$$= \frac{1}{2}\sum_{i,j,k,l}\Re\left\{\left(E\{t_{ij}t_{kl}^*\} - E\{t_{ij}\}E\{t_{kl}^*\}\right) + \left(E\{t_{ij}t_{lk}^*\} - E\{t_{ij}\}E\{t_{lk}^*\}\right)\right\}, \tag{66}$$

where we have used the fact that $t_{kl} = t_{lk}^*$. Using (37), one finds that

$$\mathrm{var}\{T_{\text{EGC}}\} \approx K\left(\|\boldsymbol{h}\|_1^4\bar{b}_4 + 2M\|\boldsymbol{h}\|_1^2\bar{b}_3 + M^2\bar{b}_2\right). \tag{67}$$

Using (64) and (67), one readily obtains (29).

D. Maximal Ratio Combining detector

Using the asymptotic diagonalization (6) of $\boldsymbol{C}$, one has $\lambda_{\max}(\boldsymbol{R}^H\boldsymbol{C}\boldsymbol{R}) \approx \lambda_{\max}(\bar{\boldsymbol{R}}^H\boldsymbol{\Lambda}\bar{\boldsymbol{R}})$, where $\bar{\boldsymbol{R}} \doteq \boldsymbol{W}^H\boldsymbol{R}$. Let us suppose now that the psd $S_{xx}(\mathrm{e}^{j\omega})$ is constant over a set with support $2\pi B$ and zero elsewhere. Then, for large K, $\boldsymbol{\Lambda}$ has BK non-zero diagonal entries, which are all equal to $1/B$ (since $\mathrm{tr}\,\boldsymbol{C} = K$). Therefore

$$\lambda_{\max}(\boldsymbol{R}^H\boldsymbol{C}\boldsymbol{R}) \approx \frac{1}{B}\lambda_{\max}(\bar{\boldsymbol{R}}_{\mathcal{B}}^H\bar{\boldsymbol{R}}_{\mathcal{B}}) \tag{68}$$

where $\bar{\boldsymbol{R}}_{\mathcal{B}}$ is a $BK \times M$ matrix comprising the rows of $\bar{\boldsymbol{R}}$ corresponding to the non-zero diagonal elements of $\boldsymbol{\Lambda}$. Note that $\bar{\boldsymbol{R}}_{\mathcal{B}}^H \bar{\boldsymbol{R}}_{\mathcal{B}}$ is a complex Wishart matrix [26], and thus under $\mathcal{H}_0$ the random variable

$$\Phi \doteq \frac{1}{\nu}\left(\frac{\lambda_{\max}(\boldsymbol{R}^H \boldsymbol{C} \boldsymbol{R})}{K} - \mu\right) \tag{69}$$

asymptotically (in K and M) follows a Tracy-Widom distribution [27], with scale and bias terms given respectively by

$$\mu = (\sqrt{BK-1} + \sqrt{M})^2, \tag{70}$$

$$\nu = (\sqrt{BK-1} + \sqrt{M})\left(\frac{1}{\sqrt{BK-1}} + \frac{1}{\sqrt{M}}\right)^{1/3}. \tag{71}$$

On the other hand, under $\mathcal{H}_1$, the random matrix $\boldsymbol{R}^H \boldsymbol{C} \boldsymbol{R} \approx \frac{1}{B} \bar{\boldsymbol{R}}_{\mathcal{B}}^H \bar{\boldsymbol{R}}_{\mathcal{B}}$ follows a spiked population model [28], i.e. all but one of the eigenvalues of the true covariance matrix $E\{\bar{\boldsymbol{R}}_{\mathcal{B}}^H \bar{\boldsymbol{R}}_{\mathcal{B}}\}$ are equal. If we denote

$$\lambda_1 \doteq \frac{1}{K}\lambda_{\max}\left(E\{\boldsymbol{R}^H \boldsymbol{C} \boldsymbol{R}\}\right) = 1 + \bar{b}_2 M \rho, \tag{72}$$

then we have that, for $\lambda_1 > 1 + \sqrt{M/K}$, the distribution of $\frac{1}{K}\lambda_{\max}(\boldsymbol{R}^H \boldsymbol{C} \boldsymbol{R})$ is given by [16], [28]

$$\frac{1}{K} T_{\text{MRC}} \sim \mathcal{N}\left(\lambda_1 + \frac{M\lambda_1}{K(\lambda_1 - 1)},\ \lambda_1^2/K\right), \tag{73}$$

asymptotically in K and M. Note that this distribution depends only on ρ and not on the spherical component $\bar{\boldsymbol{h}}$.